Generalized Partial Element Equivalent Circuit (PEEC) Modeling With Radiation Effect

Lap K. Yeung, *Member, IEEE*, and Ke-Li Wu, *Fellow, IEEE*

***Abstract*—In this paper, a new frequency-domain formulation of the partial element equivalent circuit (PEEC) model incorporating the concept of generalized complex partial inductance and pure real capacitance is introduced for modeling of 3-D structures, to which the radiation effect is not negligible. Unlike conventional PEEC-based models, the proposed formulation accounts for the radiation effect by introducing physically meaningful complex-valued inductors and pure real-valued capacitors. In essence, the imaginary part of such an inductor represents a frequency-dependent radiation resistance. Having introduced the complex inductance, there is no inversion of the complex matrix of coefficients of potential, which is not physically meaningful and inevitably creates negative resistance. It is proven in this paper that the imaginary part of the generalized complex inductance for a short dipole exactly reflects the radiation resistance of the dipole. Several numerical examples are given to validate the proposed theory. The results obtained are in good agreement with those from commercial full-wave EM solvers, showing the potential of this technique for analyzing and designing high-frequency and high-speed electronic devices.**

***Index Terms*—Antenna, partial element equivalent circuit (PEEC), partial inductance, radiation resistance, signal integrity.**

I. Introduction

As THE data rate increases to tens of gigabits per second in digital communication chips and systems, the correct prediction of electrical performances, e.g., crosstalk interference and signal integrity, for printed circuit board layouts, bonding wires, and other types of interconnects and packages becomes more and more critical to designers. Accurate modeling of these electrical characteristics requires a full-wave description of various electromagnetic (EM) wave phenomena, including mutual couplings, signal retardation, as well as conductor and substrate losses. A full-wave description would never be complete without considering the radiation effect, one of the most significant EM phenomena that must be taken into account in simulating high-speed or high-frequency circuits. In addition to the circuit modeling problems, an effective characterization of interactions between an antenna, particularly an electrically small antenna integrated in a wireless terminal, and its surrounding circuitries also requires a sophisticated modeling scheme that is suitable for time-domain simulations.

Most of the signal integrity analyses rely heavily on time-domain simulations. It is known that the most effective and dominant solver for analyzing linear and nonlinear circuit systems is SPICE. Considering the complexity of an interconnection and packaging problem, not only in terms of geometric attributes, but also the electrical size of the structure, and the compatibility among the EM physical model, nonlinear devices, and lumped element circuits in a SPICE-like solver, the most promising modeling tool would be the partial element equivalent circuit (PEEC) model [1], [2], which is a mesh-based network representation of resistors, capacitors, and inductors converted from the mixed potential integral equation (MPIE) for a given physical circuit layout.

Although the PEEC model has been used for analyzing a wide range of EM problems [3]–[11], including EM compatibility, EM interference, as well as signal integrity for high-speed electronic circuits, the radiation effect has not been successfully considered in frequency-domain modeling. There is a time-domain scheme that uses time-retarded controlled sources [12]–[16] and describes the time-delay of retarded signal traveling from one mesh element to another, although the approach is only applicable to free-space cases. Additionally, unlike the PEEC models in the frequency domain to which an effective model order reduction method can be applied [17], it is difficult to reduce the order of a time-domain PEEC model. An attempt has been made to take into account the frequency dependence of the Green's function in a frequency-domain PEEC model using the concept of complex inductance and capacitance (*LC*) in a straightforward way. However, it is inevitable to generate the negative shunt resistor, in a complex-*LC* PEEC model if the radiation effect is noticeable. This limitation restricts the use of such a PEEC model in a SPICE-like simulator for a time-domain simulation, as negative resistors will cause instability. It can be proven, with the new theory proposed in this paper, that the PEEC model with complex inductance and capacitance cannot accurately reflect the radiation effect. The rationale behind this is that the complex capacitance network obtained by inverting the matrix of complex coefficients of potential violates the stipulation that capacitance is defined only for a conservative electric field.

In this paper, a new generalized PEEC formulation is proposed for a network representation of a general EM problem with an accurate description of not only inductive and capacitive couplings, but also the radiation effect. In this frequency-domain formulation, the concept of generalized complex partial

Manuscript received February 17, 2011; revised June 26, 2011; accepted July 21, 2011. Date of publication August 30, 2011; date of current version October 12, 2011. This work was supported by the University Grants Committee of the Hong Kong Special Administrative Region under Grant AoE/P-04/08 and by the Research Grants Council of the Hong Kong Special Administrative Region under Grant 418009.

The authors are with the Department of Electronic Engineering, The Chinese University of Hong Kong, Shatin, NT, Hong Kong (e-mail: lkyeung@ee.cuhk.edu.hk; klwu@ee.cuhk.edu.hk).

Color versions of one or more of the figures in this paper are available online at http://ieeexplore.ieee.org.

Digital Object Identifier 10.1109/TMTT.2011.2163803

inductance, of which the imaginary part takes account for the radiation loss by means of a frequency-dependent resistance, is introduced for the first time. The contributions to the radiation effect from both the original "capacitance" and "inductance" terms in the MPIE are incorporated in a generalized complex inductance term. Consequently, the coefficients of potential in this new formulation are obtained from the static portion of the full-wave potential Green's function, and therefore are physically sensible. As a result, the resultant capacitance network complies with the definition of capacitance for a conservative electric field. To justify the proposed theory, it will be proven that, for a short electric dipole in free space, the extracted contribution to the radiation effect in the proposed PEEC model is exactly the same as the radiation resistance of a short dipole antenna learnt in the classical antenna theory. Furthermore, the relation between the two types of inductance of the two PEEC models, namely, the complex-*LC* model and the proposed new formulation, is also given, and from which their essential difference can be derived. Finally, to validate the new theory, a number of numerical examples, including a thin-strip dipole antenna, folded dipole antenna, patch antenna, and pair of bended differential lines, will also be discussed in detail.

II. Theory

A. Conventional PEEC Model

The PEEC model was originally developed for modeling of 3-D multiconductor systems. It is based on the transformation of the MPIE to a circuit network representation. By using a specific meshing scheme, a multiconductor structure of interest is converted to a network consisting of discrete resistors, self-inductors, and mutual inductors, as well as self-capacitors and mutual capacitors, which are called partial elements. This network results in an electromagnetically accurate equivalent-circuit model in which additional active circuit components, such as transistors, can easily be included. The partial elements are first calculated by using either numerical integration or analytical closed-form formulas [18]. The overall equivalent circuit is then solved by a conventional circuit solver.

To reveal the physical principle behind the PEEC model, it is better to derive the PEEC model based on the frequency-domain MPIE, which is given by

$$\mathbf{E}(\mathbf{r}) = -j\omega \int_{V'} \overline{\overline{G^A}}(\mathbf{r},\mathbf{r}')\cdot\mathbf{J}(\mathbf{r}')dv' - \nabla \int_{V'} G^{\phi}(\mathbf{r},\mathbf{r}')\rho(\mathbf{r}')dv' \tag{1}$$

where $\overline{\overline{G^A}}$ and G^{Φ} are the dyadic and scalar Green's functions for magnetic vector and electric scalar potentials, respectively. For the purpose of clarity, only multiconductor structures of infinitely thin metal strips embedded in free space are considered in this work. In this case, (1) can be simplified to

$$\mathbf{E}(\mathbf{r}) = -j\omega \int_{S'} \frac{\mu_0 e^{-jkR}}{4\pi R}\mathbf{J}(\mathbf{r}')ds' - \nabla \int_{S'} \frac{e^{-jkR}}{4\pi\varepsilon_0 R}\rho(\mathbf{r}')ds' \tag{2}$$

where R is the distance between the observation point $\mathbf{r}$ and the source point $\mathbf{r}'$. In addition, without loss of generality, only the x-component in (2) is considered in the following derivation. By separately discretizing the current and charge densities using rectangular pulse functions, and having $\mathbf{r}$ resided on the conducting strips, one can obtain

$$\frac{J_x(\mathbf{r})}{\sigma} = -j\omega \sum_m \left(\int_{S'_m} \frac{\mu_0 e^{-jkR}}{4\pi R} ds'_m\right) J_x^m - \frac{d}{dx}\sum_n \left(\int_{S'_n} \frac{e^{-jkR}}{4\pi\varepsilon_0 R} ds'_n\right)\rho_n. \tag{3}$$

With this discretized equation, a system of M equations is obtained by performing the Galerkin's matching procedure on (3) as

$$\frac{l_l}{\sigma w_l} I_x^l + \sum_m \frac{j\omega}{w_l w_m}\left(\iint \frac{\mu_0 e^{-jkR}}{4\pi R} ds'_m ds_l\right) I_x^m + \sum_n \frac{d}{dx}\left(\frac{1}{w_l a_n}\iint \frac{e^{-jkR}}{4\pi\varepsilon_0 R} ds'_n ds_l\right) Q_n = 0 \tag{4}$$

for $l = 1,\ldots,M$ where M is the number of inductive meshes. Notice that those pulse functions used for discretizing the current density are chosen to be the testing functions in this matching operation. Here, the integration domains have been dropped for clarity. Whereas symbols w_l and w_m are the widths of inductive meshes l and m, respectively, a_n is the area of capacitive mesh n. It is worth mentioning that (4) can be interpreted as the Kirchhoff's voltage law (KVL). The terms on the left-hand side (LHS) represents, respectively, the resistive, inductive, and capacitive voltage drops across the matched inductive mesh l. In a more circuit-oriented form, (4) can be rewritten as (subscript x is dropped from now on)

$$R_l I_l + \sum_m j\omega L_{l,m} I_m + \sum_n \left(pp_{l,n}^{+} - pp_{l,n}^{-}\right) Q_n = 0 \tag{5}$$

where a finite-difference approximation has been used for the derivative operation appearing at the last term. It will be shown in Sections II-B and II-C that both $L_{l,m}$ and $pp_{l,n}$ can be modified in a way that the radiation effect can be handled in a rigorous way.

B. Quasi-Static Capacitance

The third term in (5) represents the potential difference between the two ends of inductive mesh l (or the two capacitive meshes associated to this mesh) induced by all charges. In fact, the potentials and charges of all capacitive meshes are linked together through a system of N linear equations of

$$\Phi_i = \sum_n pp_{i,n} Q_n, \qquad \text{for } i = 1,\ldots,N \tag{6}$$

where N is the number of capacitive meshes and the coefficient of potential between two capacitive meshes i and n is defined as

$$pp_{i,n} = \frac{1}{a_i a_n}\iint \frac{e^{-jkR}}{4\pi\varepsilon_0 R} ds'_n ds_i. \tag{7}$$

Conventionally, when $kR \ll 1$, one may assume $e^{-jkR} \approx 1$ and invert (6) to obtain the short-circuited capacitances $c_{i,n}$'s.

Since $pp_{i,n}$ is, in general, a complex number for a full-wave analysis, $c_{i,n}$ may as well be a complex number. The obvious attempt to deal with this situation is to allow complex capacitances. In fact, complex capacitance can be interpreted as a capacitor in shunt with a resistor. However, in this case, the obtained complex capacitance does not have a simple physical meaning like the one in the (quasi-) static case. Indeed, it is physically meaningless since its associated shunt resistance is in general negative (assuming no dielectric loss). Alternatively, the use of physically meaningless complex capacitance can be avoided by extracting the (quasi-) static portion of (7) for the short-circuited capacitance matrix calculation. Mathematically, this can be done by separating the integral of the coefficient of potential into two parts as

$$\begin{aligned} pp_{i,n} &= pp_{i,n}^0 + pp_{i,n}^f \\ &= \frac{1}{a_i a_n} \iint \frac{1}{4\pi\varepsilon_0 R} ds'_n ds_i \\ &\quad + \frac{1}{a_i a_n} \iint \frac{e^{-jkR} - 1}{4\pi\varepsilon_0 R} ds'_n ds_i. \end{aligned} \tag{8}$$

The first integral in (8) is the conventional (quasi-) static coefficient of potential from which the real-valued short-circuited capacitance matrix can be obtained. Therefore, one can generate the capacitive portion of the PEEC model by the same token as that for (quasi-) static problems. On the other hand, the frequency-dependent second integral is not used for obtaining the capacitance network, but rather is used for generating the inductance network.

C. Generalized Complex Inductance

From (4) and (5), the mutual inductance between two inductive meshes l and m is given by

$$L_{l,m} = \frac{1}{w_l w_m} \iint \frac{\mu_0 e^{-jkR}}{4\pi R} ds'_m ds_l. \tag{9}$$

Again, it is generally a complex number. As there is no matrix inversion involved here, the imaginary part does produce a meaningful positive self-resistance ($l = m$). This complex inductance can be further generalized by "absorbing" the second integral in (8). Considering the mesh schematic shown in Fig. 1, for each inductive mesh, there should be two capacitive meshes, namely, n_1 and n_2, connecting to its ends. By applying the continuity equation on both Q_{n1} and Q_{n2} such that

$$-j\omega Q_{n1} = I_m + \sum_k I_k \tag{10a}$$

$$-j\omega Q_{n2} = -I_m + \sum_k I_k \tag{10b}$$

where ΣI_k denotes all other currents flowing into or out of either mesh node n_1 or n_2 and they are not required in the following derivation. Inserting (10) into (5), one can find a more general complex inductance as

$$\overline{L}_{l,m} = L_{l,m} + \frac{pp_{l,n1}^{f+}}{\omega^2} - \frac{pp_{l,n1}^{f-}}{\omega^2} - \frac{pp_{l,n2}^{f+}}{\omega^2} + \frac{pp_{l,n2}^{f-}}{\omega^2}. \tag{11}$$

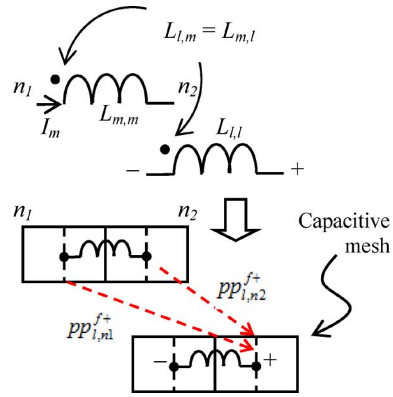

Fig. 1. Coupling configuration between inductors l and m.

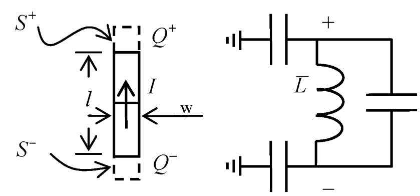

Fig. 2. Short dipole and its corresponding PEEC model.

Equation (11) reveals the relation between the inductance in the complex-*LC* PEEC model and the newly introduced generalized inductance. The significance of introducing such generalized inductance is that it can correctly account for the radiation effect from both inductive and capacitive elements virtually without any approximation. Furthermore, it completely avoids generating negative resistance in the capacitive network of the PEEC model.

D. Physical Interpretation

The imaginary part of the generalized self-inductance ($l = m$) defined in (11) contains clear physical meaning about the radiation characteristics of the corresponding inductive and capacitive elements. It, indeed, represents the overall radiation resistance of these elements. To prove this statement, a simple example, namely, a short thin-strip dipole with two opposite charge cells at each end (Fig. 2) is examined first. It is assumed that only one inductive mesh (solid rectangle) and two capacitive meshes (dashed rectangles) are used, in the lossless case, (4) takes the form of

$$\begin{aligned} &\frac{j\omega\mu_0 I}{4\pi w^2} \iint \frac{e^{-jkR}}{R} ds' ds \\ &\quad + \frac{1}{4\pi\varepsilon_0} \frac{d}{dr} \left[\frac{Q^-}{wS^-} \iint \frac{e^{-jkR}}{R} ds' ds \right. \\ &\quad \left. + \frac{Q^+}{wS^+} \iint \frac{e^{-jkR}}{R} ds' ds \right] = 0. \end{aligned} \tag{12}$$

where w is the dipole strip width and $S^{\pm}$ and $Q^{\pm}$ are the surface areas and total charges at the two ends, respectively. Notice that the integrations in (12) should be carried over their respective domains. Now, using the finite-difference approach for the derivative operation and (11), the generalized self-inductance $\overline{L}$ can be obtained as

$$\overline{L} = \frac{\mu_0}{4\pi w^2}\iint \frac{e^{-jkR}}{R}ds'ds + \frac{pp_-^{f+}}{\omega^2} - \frac{pp_-^{f-}}{\omega^2} - \frac{pp_+^{f+}}{\omega^2} + \frac{pp_+^{f-}}{\omega^2} \tag{13}$$

where the four frequency-dependent coefficients of potential are given by

$$pp_-^{f+} = \frac{1}{4\pi\varepsilon_0 S^-}\int_{S^-} \frac{e^{-jkR^+}-1}{R^+}ds' \tag{14a}$$

$$pp_-^{f-} = \frac{1}{4\pi\varepsilon_0 S^-}\int_{S^-} \frac{e^{-jkR^-}-1}{R^-}ds' \tag{14b}$$

$$pp_+^{f+} = \frac{1}{4\pi\varepsilon_0 S^+}\int_{S^+} \frac{e^{-jkR^+}-1}{R^+}ds' \tag{14c}$$

$$pp_+^{f-} = \frac{1}{4\pi\varepsilon_0 S^+}\int_{S^+} \frac{e^{-jkR^-}-1}{R^-}ds' \tag{14d}$$

where R^+ and R^- are defined as $|\mathbf{r}^+ - \mathbf{r}'|$ and $|\mathbf{r}^- - \mathbf{r}'|$, respectively. To find a good approximation of the integrals in (13) and (14) analytically, the Taylor's series expansion of

$$\frac{e^{-jkR}}{R} = \frac{1}{R} - jk - \frac{k^2R}{2!} + \frac{jk^3R^2}{3!} + \cdots \tag{15}$$

can be used. Substituting (15) into the first integral in (13), the original complex inductance term becomes

$$\frac{\mu_0}{4\pi w^2}\iint \frac{e^{-jkR}}{R}ds'ds \approx \frac{\mu_0}{4\pi w^2}\iint \frac{1}{R}ds'ds - \frac{j\mu_0 kl^2}{4\pi}. \tag{16}$$

Here, only the first two terms of the Taylor's expansion are used since $kR \ll 1$. In a similar manner, the frequency-dependent coefficients of potential in (14) can be approximated, respectively, by

$$pp_-^{f+} \approx \frac{-jk}{4\pi\varepsilon_0} - \frac{1}{4\pi\varepsilon_0 S^-}\int_{S^-} \frac{k^2R^+}{2!} - \frac{jk^3(R^+)^2}{3!}ds' \tag{17a}$$

$$pp_-^{f-} \approx \frac{-jk}{4\pi\varepsilon_0} \tag{17b}$$

$$pp_+^{f+} \approx \frac{-jk}{4\pi\varepsilon_0} \tag{17c}$$

$$pp_+^{f-} \approx \frac{-jk}{4\pi\varepsilon_0} - \frac{1}{4\pi\varepsilon_0 S^+}\int_{S^+} \frac{k^2R^-}{2!} - \frac{jk^3(R^-)^2}{3!}ds'. \tag{17d}$$

Notice that only the first two terms in the Taylor's expansion are used for obtaining (17b) and (17c), whereas the first four terms are required for (17a) and (17d) because the kR term in these two equations is relatively larger than the one in the "self"-coefficients of (17b) and (17c).

By assuming $R^+ = R^- \approx l$, the equations in (17) can be further simplified and the final expression of the generalized self-inductance $\overline{L}$ is

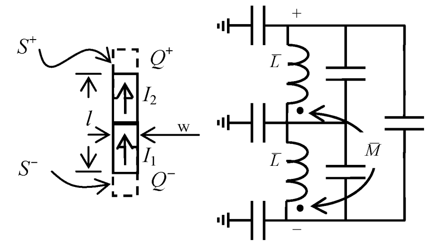

Fig. 3. Two-inductive-element configuration of a short dipole.

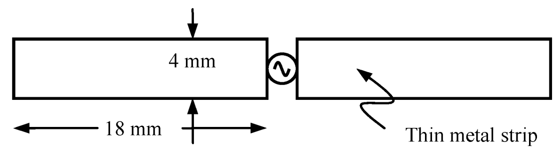

Fig. 4. Thin-strip half-wavelength dipole antenna.

$$\overline{L} = \frac{\mu_0}{4\pi w^2}\iint \frac{1}{R}ds'ds - \frac{\mu_0 l}{4\pi} - j\left(\frac{\mu_0 kl^2}{6\pi}\right). \tag{18}$$

The real part of $j\omega\overline{L}$ can be interpreted as a frequency-dependent resistance with the value of

$$R = 80\pi^2\left(\frac{l}{\lambda}\right)^2 \tag{19}$$

which is exactly the same as the well-known radiation resistance of a short dipole with a uniform current distribution. The same result can be obtained for the meshing configuration consisting of two inductive and three capacitive elements. Although only the final expressions are presented here, the detailed derivation is given in the Appendix. The equivalent circuit under such meshing scheme is shown in Fig. 3. The expressions for the generalized self- and mutual inductances are given by

$$\overline{L} = \frac{\mu_0}{4\pi w^2}\iint \frac{1}{R}ds'ds - \frac{\mu_0 l}{8\pi} - j\left(\frac{\mu_0 kl^2}{24\pi}\right) \tag{20}$$

$$\overline{M} = \frac{\mu_0}{4\pi w^2}\iint \frac{1}{R}ds'ds - j\left(\frac{\mu_0 kl^2}{24\pi}\right). \tag{21}$$

If the current is uniformly distributed on the dipole (i.e., the currents on both inductors are the same), then the total series resistance is given by the real part of $2j\omega\overline{L} + 2j\omega\overline{M}$, which is again equal to (19).

III. Numerical Examples

A. Thin-Strip Half-Wavelength Dipole Antenna

The first example to be studied is a simple thin-strip half-wavelength dipole antenna shown in Fig. 4. The dipole is excited at the center by a lumped power port of impedance 50 Ω. In the proposed PEEC formulation, the thin dipole is divided into 72 capacitive and 114 inductive elements, corresponding to a

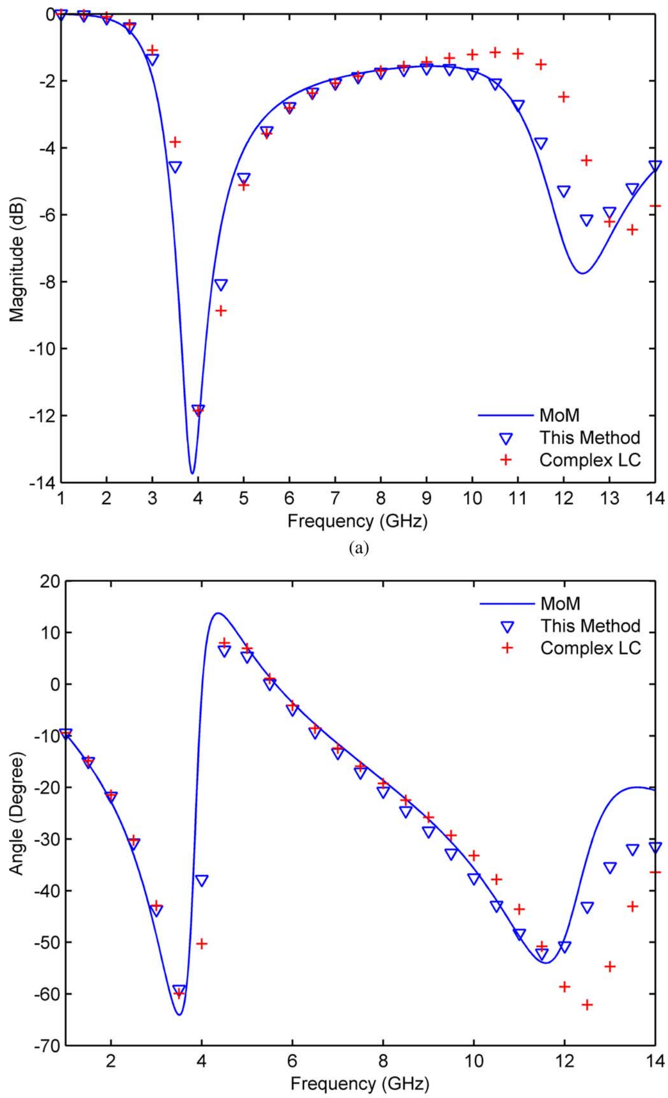

(a)

(b)

Fig. 5. Simulated results (S_{11}) for the thin-strip dipole. (a) Magnitude. (b) Phase.

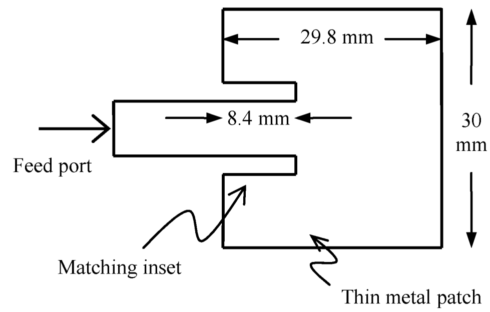

Fig. 6. Air-filled patch antenna.

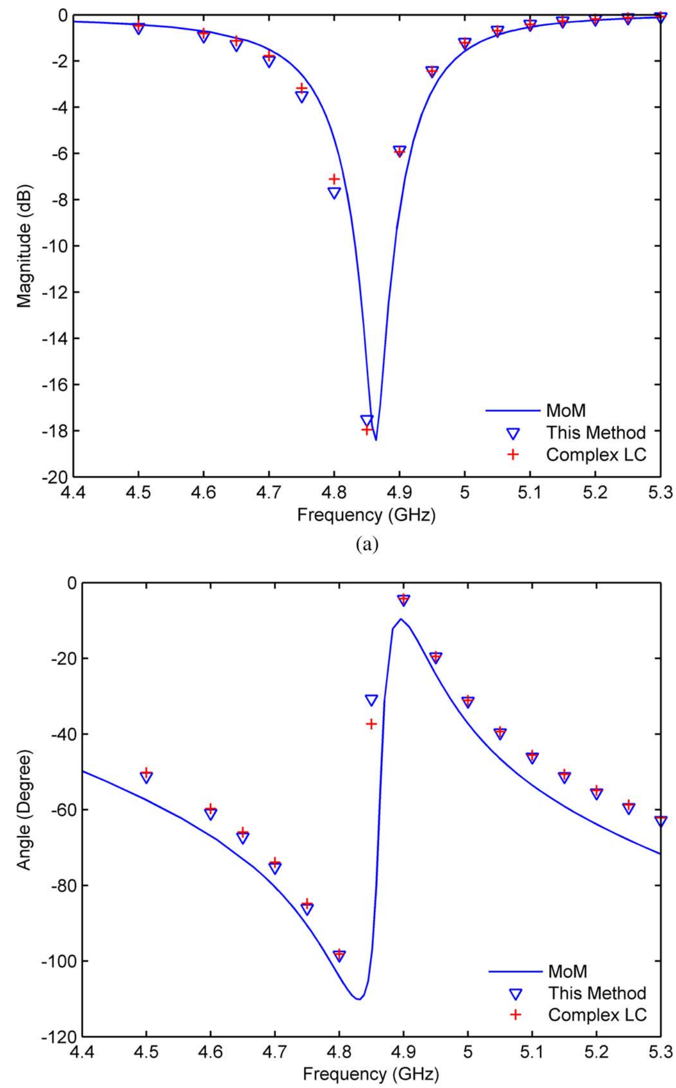

(a)

(b)

Fig. 7. Simulated results (S_{11}) for the air-filled patch. (a) Magnitude. (b) Phase.

scheme of 20 meshes per wavelength at 10 GHz. Simulated scattering parameters from the method of moments (MoM)-based full-wave solver, Momentum of Agilent EEsof, and those from the two mentioned PEEC-based methods are depicted in Fig. 5. It is seen that the dipole antenna exhibits a series resonance at around 3.8 GHz and acts as a half-wave dipole antenna. Since the port definitions for the two models are different, some small discrepancies can be seen from the results of the MoM model and the PEEC models. However, in general, they agree well.

One particularly interesting fact is that there are slight differences between the results by the PEEC model with complex inductance and capacitance and those obtained by the proposed PEEC model at high frequencies (>10 GHz) where the radiation effect is more obvious.

B. Air-Filled Patch Antenna

The second example is an air-filled patch antenna and its geometry is depicted in Fig. 6. The patch is 1 mm above an infinitely large ground plane. The antenna is fed by a microstrip with an inset dimension of 8.4- and 1-mm line-to-radiator spacing so as to match to an impedance of 50 Ω. The geometry is divided into a total of 168 capacitive and 301 inductive elements, corresponding to a scheme of 20 meshes per wavelength at 5.4 GHz. From the simulated results, as given in Fig. 7, it is seen that the patch operates at around 4.9 GHz. At low frequencies, the scattering parameters calculated by the MoM-based solver are

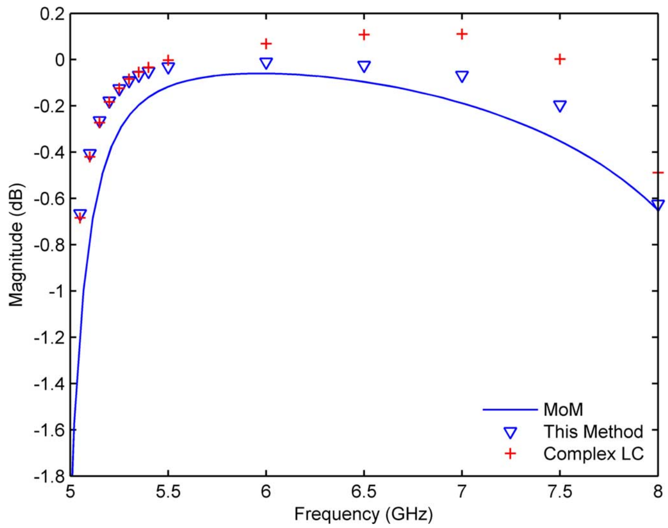

Fig. 8. Simulated $|S_{11}|$ for the air-filled patch at higher frequencies.

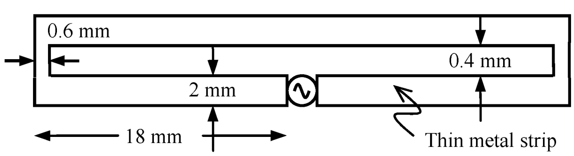

Fig. 9. Geometry for the thin-strip folded-dipole example.

closer to those obtained by the two PEEC-based methods. However, at frequencies greater than 5.5 GHz, as shown in Fig. 8, the complex-*LC* PEEC model gives less accurate results and even produces positive $|S_{11}|$ in decibels. This gain effect is caused by the negative shunt resistors, which are obtained by inverting the complex coefficients of potential matrix, in the associated PEEC model.

C. Thin-Strip Folded-Dipole Antenna

The third example to be considered is a thin-strip folded dipole, which is depicted in Fig. 9. It is composed of two infinitely thin metal strips that are connected at both ends. The dipole is excited at the center of the primary strip by a lumped power port. Since the port impedance of a folded dipole is theoretically four times that of a conventional dipole, the lumped port impedance is thus selected to be 200 Ω. The geometry is meshed with a scheme of 30 meshes per wavelength at 10 GHz for the PEEC-based modeling. This corresponds to a total of 164 capacitive meshes and 241 inductive meshes. All simulation results show that the dipole operates around 3.8 GHz, which is the same as the first example. Again, the proposed method is superior to the PEEC method with complex inductance and capacitance in the high-frequency range, as presented in Fig. 10.

D. Pair of 90° Bended Differential Lines

The final example is used to demonstrate the significance of the radiation effect on high-speed circuit traces. In Fig. 11, the geometric configuration for a section of 90° bended 100-Ω differential line is depicted. This line consists of two thin metal

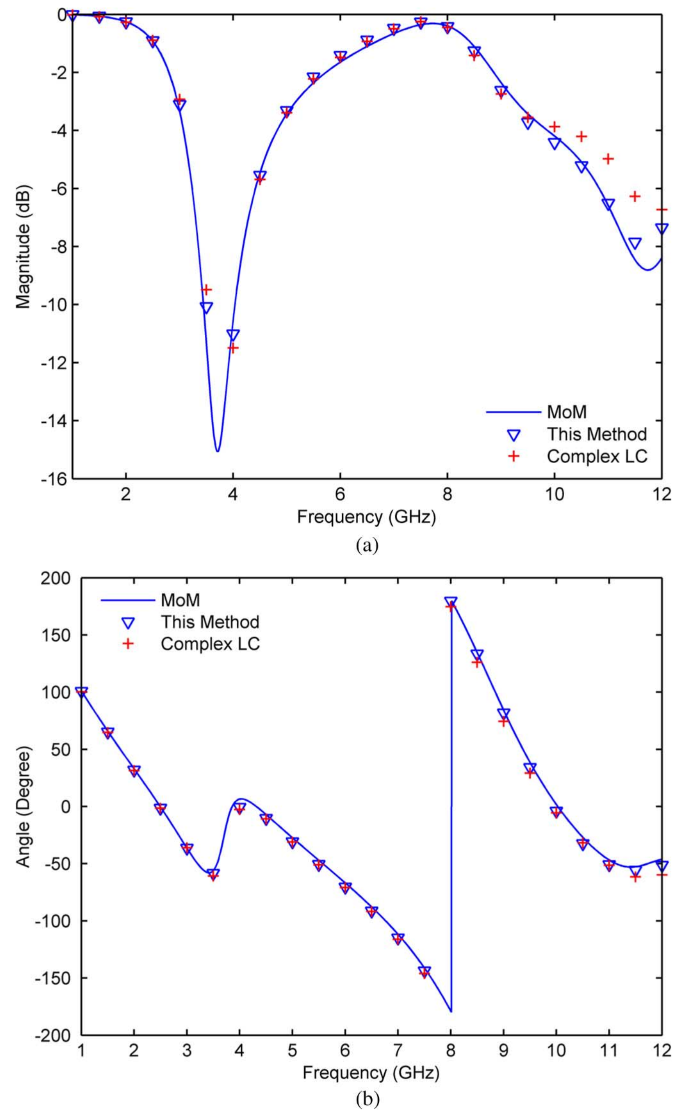

Fig. 10. Simulated results (S_{11}) for the folded dipole. (a) Magnitude. (b) Phase.

strips of 0.6-mm width separated by a gap of 0.2 mm. It is suspended in a homogeneous substrate of dielectric constant 4.3. In the PEEC-based analyses, it is discretized with 25 meshes per wavelength at 20 GHz. This corresponds to 124 capacitive and 182 inductive elements. It is known that any kind of discontinuity would induce radiation, particularly at high frequencies, at which conventional (quasi-) static assumption is simply not valid. This perception is confirmed by the dashed curves shown in Fig. 12, in which the results obtained from the (quasi-) static PEEC model only agree well with the MoM-based solutions at frequencies below 6 GHz. On the other hand, the proposed PEEC model and PEEC model with complex inductance and capacitance can reach to higher frequencies with the former producing more accurate results.

IV. Conclusion

A new PEEC formulation, which incorporates generalized complex inductance and pure real capacitance, has been pro-

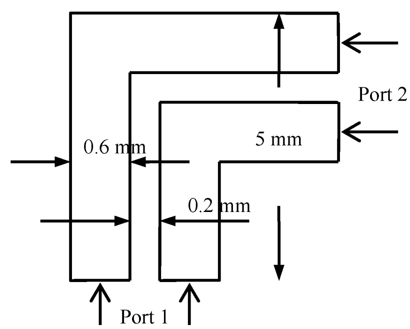

Fig. 11. Geometry for the 90° bended differential line section.

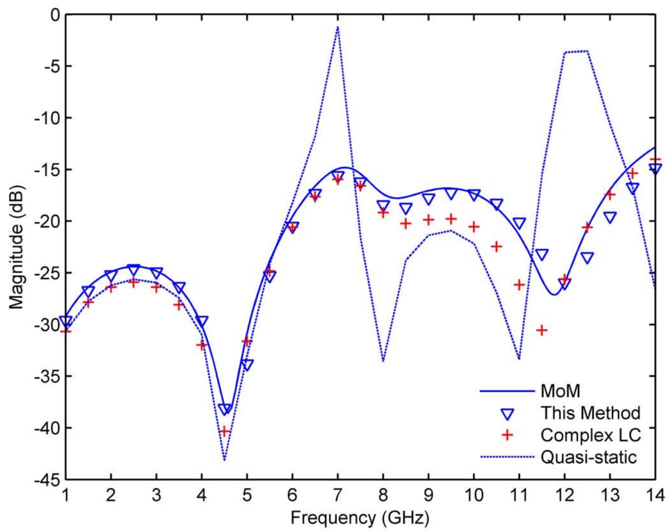

(a)

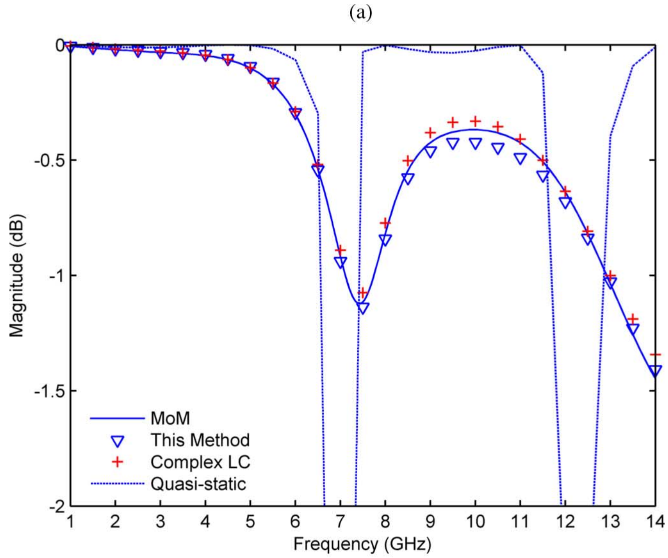

(b)

Fig. 12. Simulated s-parameter for the bended differential line section. (a)$|S_{11}|$. (b) $|S_{12}|$.

posed for modeling high-speed and high-frequency structures to which the radiation effect cannot be ignored. In this model, the radiation effect in the original "capacitance" terms is extracted and combined with that in the original "inductance" terms to form a new circuit model, the generalized complex inductance. With the use of such inductors, the conventional definition of capacitance is still applicable for calculating the capacitive components, and thus requires no physically meaningless inversion of the complex coefficients of potential matrix. Several numerical examples have been studied to validate the new formulation. It is seen from these studies that the PEEC model using the generalized complex inductors can correctly account for the radiation loss with theoretically guaranteed positive frequency-dependent resistors. Comparing to the conventional frequency-domain PEEC model, the proposed PEEC model is physically sound and numerically stable. The new PEEC model lays a good foundation for a legitimate model order reduction in the frequency domain.

APPENDIX
DERIVATION OF THE TWO-INDUCTIVE-ELEMENT DIPOLE MODEL

For the two-inductive-element configuration shown in Fig. 3, the self-inductance (L) and mutual inductance (M) can be derived as

$$L = \frac{\mu_0}{4\pi w^2}\iint \frac{1}{R} ds' ds - \frac{j\mu_0 k l^2}{16\pi} \quad \text{(A1)}$$

$$M = \frac{\mu_0}{4\pi w^2}\iint \frac{1}{R} ds' ds - \frac{j\mu_0 k l^2}{16\pi}. \quad \text{(A2)}$$

Notice that although the two expressions are identical, the integration domains for (A1) and (A2) are different and the imaginary part of L is four times smaller than that of (16) because the inductive elements are now halved in length. At the same time, the scalar potential at the center of the dipole is given by

$$\phi^c = \frac{Q^c}{4\pi\varepsilon_0 S^c}\int_{S^c} \frac{e^{-jkR^c}}{R^c} ds' + \frac{Q^+}{4\pi\varepsilon_0 S^+}\int_{S^+} \frac{e^{-jkR^c}}{R^c} ds' + \frac{Q^-}{4\pi\varepsilon_0 S^-}\int_{S^-} \frac{e^{-jkR^c}}{R^c} ds' \quad \text{(A3)}$$

and the scalar potential at the lower end of the dipole is

$$\phi^- = \frac{Q^c}{4\pi\varepsilon_0 S^c}\int_{S^c} \frac{e^{-jkR^-}}{R^-} ds' + \frac{Q^+}{4\pi\varepsilon_0 S^+}\int_{S^+} \frac{e^{-jkR^-}}{R^-} ds' + \frac{Q^-}{4\pi\varepsilon_0 S^-}\int_{S^-} \frac{e^{-jkR^-}}{R^-} ds' \quad \text{(A4)}$$

where R^c and R^- are the distance between $\mathbf{r}'$ and the dipole center, and $\mathbf{r}'$ and the dipole lower end, respectively. Using the Taylor's series expansion of (15), the frequency-dependent potential difference between the center and the lower end can be simplified to

$$\phi^c - \phi^- = \frac{Q^c}{4\pi\varepsilon_0}\left(\frac{k^2 l}{4} - \frac{jk^3 l^2}{24}\right) + \frac{Q^+}{4\pi\varepsilon_0}\left(\frac{k^2 l}{4} - \frac{j3k^3 l^2}{24}\right) + \frac{Q^-}{4\pi\varepsilon_0}\left(-\frac{k^2 l}{4} + \frac{jk^3 l^2}{24}\right). \quad \text{(A5)}$$

Now, replacing the charges with currents in a similar way as that listed in (10), and using (5) and (A1) and (A2), the generalized self-inductances and mutual inductances can then be obtained as given in (20) and (21), respectively.

REFERENCES

[1] A. E. Ruehli, "Inductance calculations in a complex integrated circuit environment," *IBM J. Res. Develop.*, vol. 16, pp. 470–481, Sep. 1972.

[2] A. E. Ruehli, "Equivalent circuit models for three dimensional multiconductor systems," *IEEE Trans. Microw. Theory Tech.*, vol. MTT-22, no. 3, pp. 216–221, Mar. 1974.

[3] H. H. Heeb and A. E. Ruehli, "Three-dimensional interconnect analysis using partial element equivalent circuits," *IEEE Trans. Circuits Syst.*, vol. 39, no. 11, pp. 974–982, Nov. 1992.

[4] A. E. Ruehli, "Circuit models for three-dimensional geometries including dielectrics," *IEEE Trans. Microw. Theory Tech.*, vol. 40, no. 7, pp. 1507–1516, Jul. 1992.

[5] H. Shi, J. Fan, and J. Drewniak, "Modeling multilayered PCB power-bus designs using an MPIE based circuit extraction technique," in *Proc. IEEE Int. EMC Symp.*, Denver, CO, 1998, pp. 647–651.

[6] L. Chang and K.-J. Chang, "Accurate and efficient inductance extraction for SoC noise and signal integrity," in *IEEE Int. Elect. Perform. Electron. Packag. Conf. Rec.*, 2002, pp. 209–213.

[7] B. Archambeault, "Analyzing power/ground plane decoupling performance using the partial element equivalent circuit (PEEC) simulation technique," in *Proc. IEEE Int. EMC Symp.*, Seattle, WA, 2000, pp. 779–784.

[8] S. A. Teo, B. L. Ooi, S. T. Chew, and M. S. Leon, "A fast PEEC technique for full-wave parameters extraction of distributed elements," *IEEE Microw. Wireless Compon. Lett.*, vol. 11, no. 5, pp. 226–228, May 2001.

[9] K.-L. Wu, L. K. Yeung, and Y. Ding, "An efficient PEEC algorithm for modeling of LTCC RF circuits with finite metal strip thickness," *IEEE Microw. Wireless Compon. Lett.*, vol. 13, no. 9, pp. 390–392, Sep. 2003.

[10] V. Vahrenholt, H. Brüns, and H. Singer, "Fast EMC analysis of systems consisting of PCBs and metallic antenna structures by a hybridization of PEEC and MoM," *IEEE Trans. Electromagn. Compat.*, vol. 52, no. 11, pp. 962–973, Nov. 2010.

[11] J. Garrett, "Advancement of the partial element equivalent circuit formulation," Ph.D. dissertation, Dept. Elect. Eng., Univ. Kentucky, Lexington, KY, 1997.

[12] J. Garrett, A. Ruehli, and C. Paul, "Accuracy and stability improvements of integral equation models using the partial element equivalent circuit (PEEC) approach," *IEEE Trans. Antennas Propag.*, vol. 46, no. 12, pp. 1824–1832, Dec. 1998.

[13] A. Ruehli *et al.*, "Nonorthogonal PEC formulation for time- and frequency-domain EM and circuit modeling," *IEEE Trans. Electromagn. Compat.*, vol. 45, no. 5, pp. 167–176, May 2003.

[14] S. Kochetov and G. Wollenberg, "Stability of full-wave PEEC models: Reason for instabilities and approach for correction," *IEEE Trans. Electromagn. Compat.*, vol. 47, no. 11, pp. 738–748, Nov. 2005.

[15] X. Zhang and Z. Feng, "A new retarded PEEC model for antenna," presented at the IEEE Asia–Pacific Microw. Conf., Hong Kong, 2008.

[16] S. Sundberg and J. Ekman, "PEEC modeling of antenna characteristics," in *Proc. IEEE Int. EMC Symp.*, Portland, OR, 2006, pp. 580–585.

[17] H. Hu, K. Yang, K.-L. Wu, and W.-Y. Yin, "Quasi-static derived physically expressive circuit model for lossy integrated RF passives," *IEEE Trans. Microw. Theory Tech.*, vol. 56, no. 8, pp. 1954–1961, Aug. 2008.

[18] C. Hoer and C. Love, "Exact inductance equations for rectangular conductors with applications to more complicated geometries," *J. Res. Nat. Bur. Stand.*, vol. 69c, pp. 127–137, Apr. 1965.

Lap K. Yeung (S'00–M'02) received the B.Eng. degree in electrical and information engineering from the University of Sydney, Sydney, Australia, in 1998, the M.Eng. degree in electronic engineering from the Chinese University of Hong Kong, Shatin, Hong Kong, in 2002, and the Ph.D. degree in electrical engineering from the University of California at Los Angeles (UCLA), in 2009.

During 1999, he was with the Commonwealth Scientific and Industrial Research Organization (CSIRO), Sydney, Australia, where he was a Research Engineer involved in the numerical modeling of different antenna structures. From 2003 to 2006, he was with the Chinese University of Hong Kong, where he is involved in various low-temperature co-fired ceramic (LTCC) multichip-module (MCM) designs and the development of numerical algorithms for analyzing multilayer embedded RF modules.

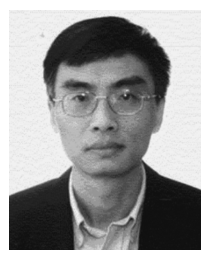

Ke-Li Wu (M'90–SM'96–F'11) received the B.S. and M.Eng. degrees from the Nanjing University of Science and Technology, Nanjing, China, in 1982 and 1985, respectively, and the Ph.D. degree from Laval University, Quebec, QC, Canada, in 1989.

From 1989 to 1993, he was with the Communications Research Laboratory, McMaster University, as a Research Engineer and Group Manager. In March 1993, he joined the Corporate Researcj and Development Division, Com Dev International, where he was a Principal Member of Technical Staff in charge of developing advanced EM design software for microwave subsystems for satellite and wireless communications. Since October 1999, he has been with the Department of Electronic Engineering, The Chinese University of Hong Kong, Shatin, Hong Kong, where he is currently a Professor. He has authored or coauthored numerous publications in the areas of EM modeling and microwave and antenna engineering. His current research interests include numerical and analytical methods in electromagnetics, passive microwave circuits, theory and practices of microwave filters, antennas for wireless terminals, low temperature co-fired ceramic (LTCC)-based multichip modules (MCMs) for wireless communications, and RF identification (RFID) technologies.